Novel Composites of TiO_2 (Anatase) and Silicate Nanoparticles

H. Y. Zhu,*,† J. A. Orthman,† J.-Y. Li,‡ J.-C. Zhao,‡ G. J. Churchman,§ and E. F. Vansant||

Department of Chemical Engineering, The University of Queensland, St Lucia, Queensland 4072, Australia, Centre for Molecular Science, Institute of Chemistry, The Chinese Academy of Science, Beijing 100080, China, CSIRO Land and Water, Private Mail Bag No. 2, Glen Osmond, South Australia 5064, Australia, and Laboratory of Adsorption and Catalysis, Department of Chemistry, University of Antwerp (U.I.A.), Universiteitsplein 1, B-2610 Wilrijk, Belgium

Received May 20, 2002. Revised Manuscript Received August 26, 2002

Thermally stable composite nanostructures of titanium dioxide (anatase) and silicate nanoparticles were prepared from Laponite clay and a sol of titanium hydrate in the presence of poly(ethylene oxide) (PEO) surfactants. Laponite is a synthetic clay that readily disperses in water and exists as exfoliated silicate layers of about 1-nm thick in transparent dispersions of high pH. The acidic sol solution reacts with the clay platelets and leaches out most of the magnesium in the clay, while the sol particles hydrolyze further due to the high pH of the clay dispersion. As a result, larger precursors of TiO_2 nanoparticles form and condense on the fragmentized pieces of the leached silicate. Introducing PEO surfactants into the synthesis can significantly increase the porosity and surface area of the composite solids. The TiO_2 exists as anatase nanoparticles that are separated by silicate fragments and voids such that they are accessible to organic molecules. The size of the anatase particle can be tailored by manipulating the experimental parameters at various synthesis stages. Therefore, we can design and engineer composite nanostructures to achieve better performance. The composite solids exhibit superior properties as photocatalysts for the degradation of Rhodamine 6G in aqueous solution.

Introduction

Titanium dioxide (TiO_2) is an important catalyst and catalyst support.[1,2] In particular, it is regarded as the best photocatalyst for decomposing refractory organic pollutants in water and air.[1,3−5] It can be used in various processes such as odor elimination from drinking water, degradation of oil spills in surface water systems, and degradation of harmful organic contaminants such as herbicides, pesticides, and refractive dyes. Ultrafine TiO_2 powders have large specific surface areas and are expected to have good catalytic activities since reactions take place on the TiO_2 surface. However, when pure TiO_2 powders are used, two main problems occur. First, ultrafine powders will agglomerate into larger particles, resulting in an adverse effect on catalyst performance. Second, it is very hard to recover pure TiO_2 powders from water when they are used in aqueous systems, leading to a potential difficulty in downstream separation.[6] Various new techniques have been adopted to develop solids that reduce such problems and still have large TiO_2 surface areas. Recently, TiO_2 mesoporous molecular sieves have been prepared by templated synthesis.[7,8] This technique was invented in the early 1990s for the synthesis of mesoporous silica and aluminosilicate.[9,10] Some approaches, such as starting with metal alkoxides and conducting the synthesis in nonaqueous systems, were employed to overcome serious difficulties in the synthesis.[7,8]

Large TiO_2 surface areas are also available in layered clays intercalated with TiO_2 particles, so-called TiO_2 pillared clays.[11,12] These composite solids have a porous structure, and thus, the TiO_2 surface is accessible for reactant molecules. The technique of pillaring clays with

* To whom correspondence should be addressed. Telephone: 61 7 3365 9058. Fax: 61 7 3365 4199. E-mail: hyzhu@cheque.uq.edu.au.
† The University of Queensland.
‡ The Chinese Academy of Science.
§ CSIRO Land and Water.
|| University of Antwerp.

(1) Fujishima, A.; Hashimoto, K.; Watanabe, T. *TiO_2 Photocatalysis Fundamentals and Applications*; BKC, Inc.: Tokyo, 1999.
(2) Kodama, S.; Nakaya, H.; Anpo, M.; Kubokawa, Y. *Bull. Chem. Soc. Jpn.* **1986**, *58*, 3645.
(3) Linsebigler, A. L.; Lu, G.; Yates, J. T., Jr. *Chem. Rev.* **1995**, *95* (3), 735.
(4) Liu, G.; Li, X.; Zhao, J.; Hidaka, H.; Serpone, N. *Environ. Sci. Technol.* **2000**, *34* (18), 3982.
(5) Anpo, M. *Pure Appl. Chem.* **2000**, *72* (7), 1265.
(6) Beydoun, D.; Amal R.; Low, G. K.-C.; McEvoy, S. *J. Phys. Chem.* **2000**, *104*, 4387.
(7) Antonelli, D. M.; Ying, J. Y. *Angew. Chem., Int. Ed. Engl.* **1995**, *34* (18), 2014.
(8) Yang, P.; Zhao, D.; Margolese, D. I.; Chmelka, B. F.; Stucky, G. D. *Nature* **1998**, *396*, 152.
(9) Kresge, C. T.; Leonowicz, M. E.; Roth, W. J.; Vartuli, J. C.; Beck, J. S. *Nature* **1992**, *359*, 710.
(10) Inagaki, S.; Fukushima, Y.; Kuroda, K. *J. Chem. Soc., Chem. Commun.* **1993**, 680.
(11) Sterte, J. *Clays Clay Miner.* **1986**, *34*, 658.
(12) Yamanaka, S.; Nishihara, T.; Hattori, M.; Suzuki, Y. *Mater. Chem. Phys.* **1987**, *17*, 87.

10.1021/cm0205884 CCC: $22.00
Published on Web 12/16/2002

metal oxide particles was invented 2 decades ago.[13,14] TiO_2 pillared clays are prepared from aqueous systems through simple procedures. The precursors of the TiO_2 particles are positively charged sol particles of titanium hydrate, $[TiO(OH)_x]_m^{n+}$, which are 1−2 nm in size and can be readily exchanged with the interlayer sodium ions of clays to form the intercalated structure.[11,12] Nevertheless, TiO_2 pillared clays are microporous solids of moderate porosity and most titanium dioxide in TiO_2 pillared clays is amorphous.[15] While TiO_2 crystal phases are important semiconductors and required for many applications, the TiO_2 pillars are too small to form a crystal phase. It is also difficult to alter the pillar's size or the pore structure of the pillared clays. These properties limit the applications of the materials.[16]

In the present study, we report the synthesis of mesoporous composite nanostructures comprising homogeneous solid dispersions of anatase and silicate nanoparticles with a very large porosity. Laponite, a synthetic layered smectite clay, was used in the synthesis. In a dilute aqueous dispersion the clay exists as discrete plates of diameter 20−30 nm.[17] Therefore, it is a good starting material for forming nanometer-scale composite structures with titania sol particles. Moreover, we can alter the size of the anatase crystals by manipulating the acid to titanium molar ratio and greatly increase the porosity of the resultant composite through introducing PEO surfactant of small molecular weight. These findings allow us to effectively tailor the structure of these solids for various applications. For instance, TiO_2 nanocomposites obtained in this study are found to be superior photocatalysts for the degradation of Rhodamine 6G in aqueous solutions, while TiO_2 pillared clays exhibit poor photocatalytic activity for the degradation of such large organic molecules (with more than 10 carbons in a molecule) because of the steric hindrance of the small pore entrances (about 1.5 nm) in TiO_2 pillared clays.[13]

Experimental Section

Materials. The Laponite clay (Laponite RD) was supplied by Fernz Specialty Chemicals, Australia, and used as received. The clay powder has a BET specific surface area of 370 m^2/g and a cation exchange capacity of 55 mequiv/100 g of clay. Titanium tetraisopropoxide $Ti(OC_3H_7)_4$, from Aldrich, was used as received without further purification to prepare the sol of titanium hydrate. Five nonionic poly(ethylene oxide) surfactants from Aldrich, Tergitol 15S-*n* (n = 5, 7, 9, 12, and 30), were used in this study. The PEO surfactants have a general chemical formula of $C_{12-14}H_{25-29}O(CH_2CH_2O)_nH$ and have relatively low average molecular weights. For example, the molecular weight of Tergitol 15S-5 (n = 5) and Tergitol 15S-12 (n = 12) are 420 and 730 g/mol, respectively. TiO_2 nanoparticulates of P25 (≈80% anatase and ≈20% rutile, BET area ≈50 m^2/g) were kindly supplied by Degussa Co., Germany.

Preparation of Samples. Laponite (4.0 g) was dispersed into 200 mL of deionized water (pH ∼ 6.5 and conductivity ≈0.06 μS/cm) and the suspension was stirred until it became transparent (≈40 min). Enough of a PEO surfactant was added into the Laponite dispersion to cause it to become opaque. To this mixture, a sol solution of titanium hydrate was added dropwise with continuous stirring. The sol of titanium hydrate was obtained by the hydrolysis of $Ti(OC_3H_7)_4$ in HCl solution and aged for 3 h.[12,15] The molar ratio of $[Ti]/[H^+]$ is 1:4. After the solution was stirred for a further 3 h, the suspension was transferred into an autoclave and maintained at 373 K for 2 days. A white precipitate was recovered from the mixture by centrifuging and washed with deionized water until it was free of Cl^- ions according to a test with $AgNO_3$. The wet cake was dried in air and calcined at 773 K for 20 h. The temperature was raised at a rate of 2 K/min. Samples were prepared with different acidity, mass ratio of surfactant to clay, mass ratio of titanium to clay (Ti/L), and a different number (n) of $-CH_2-CH_2O-$ groups.

Characterization. Transmission electron microscopy (TEM) images were taken with a JEOL 2010 microscope on powder samples deposited onto a copper microgrid coated with a holey carbon film. The elemental analysis of the samples was conducted by X-ray fluorescence (XRF) on a Philips PW 1480 spectrometer that used a wavelength dispersive technique. N_2 adsorption/desorption isotherms were measured at liquid nitrogen temperature using a gas sorption analyzer (Quantachrome, NOVA 1200). The samples were degassed at 523 K and a vacuum below 10^{-3} Torr for 16 h prior to the measurement. The specific surface area was calculated by the BET equation and the mean pore size was determined through the *t*-plot method.[18]

Thermogravimetric analysis (TGA) of the uncalcined samples was performed on a Shimazu TGA-50. About 10 mg of solid before calcination was loaded onto a platinum pan and heated from room temperature to 1173 K at a heating rate of 5 K/min in an air flow of 80 mL/min. X-ray diffraction (XRD) patterns of the powder samples were recorded on a Philips PW 1050/25 goniometer equipped with a graphite monochromator. Cu Kα radiation and a fixed power source (40 kV, 40 mA) were used. The scan rate was 1° (2θ)/min. Solid-state ^{29}Si magic-angle spinning nuclear magnetic resonance (^{29}Si MAS NMR) was recorded at 59.63 MHz on a Bruker MSL 300 spectrometer. Powder samples were spun at a frequency of 2.5 Hz in Bruker double-air-bearing probes. The CP contact time used in this study was 8 ms.

Photodegradation of Rhodamine 6G. The UV source was a 100-W Hg lamp (Toshiba SHLS-1002A). Aqueous suspensions of Rhodamine 6G (25 mL, with an initial concentration of 2×10^{-5} M) and photocatalyst powder (25 mg) were placed in a Pyrex vessel. Prior to irradiation, the suspensions were magnetically stirred in the dark for ≈30 min to establish an adsorption/desorption equilibrium between the dye and the catalyst surface. At given intervals of illumination, a specimen (3 mL) of the suspension was collected, centrifuged, and then filtered through a Millipore filter. The filtrates were analyzed by UV−Vis spectroscopy using a lambda Bio 20 spectrophotometer.

Results

Elemental Analysis. The major chemical composition of the Laponite and two TiO_2 nanocomposites are given in Table 1. Both nanocomposite samples were prepared with a $[Ti]/[H^+]$ ratio of 1:4, but one was prepared with PEO surfactant Tergitol 15S-7 (the ratio of PEO/Laponite of 2:1) and the other was prepared without surfactant.

The TiO_2 nanocomposite samples were calcined at 773 K and contain mainly silica and titanium dioxide. Substantial ignition losses are due to moisture, adsorbed CO_2, and organics on the samples. Compared with that

(13) Burch, R., Ed. *Pillared Clays*, *Catalysis Today*; Elsevier: New York, 1988; Vols. 2 and 3.
(14) Pinnavaia, T. J. *Science* **1983**, *220*, 365.
(15) Ding, Z.; Zhu, H. Y.; Lu, G. Q.; Greenfield, P. F. *J. Colloid Interface Sci*. **1999**, *209*, 193.
(16) Yoneyama, H.; Haga, S.; Yamanaka, S. *J. Phys. Chem*. **1989**, *93*, 4833.
(17) Thompson, D. W.; Butterworth: J. T. *J. Colloid Interface Sci*. **1992**, *151* (1), 236.
(18) Zhu, H. Y.; Zhao, X. S.; Lu, G. Q.; Do, D. D. *Langmuir* **1996**, *12* (26), 6513.

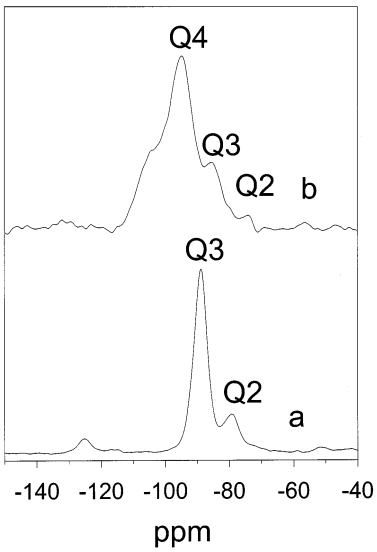

Figure 1. ^{29}Si magic-angle spinning nuclear magnetic resonance (^{29}Si MAS NMR) of the samples. (a) is the spectrum for Laponite clay and (b) the spectrum for the TiO_2 nanocomposite prepared with the surfactant Tergitol 15S-7, a [Ti]/[H^+] ratio of 1:4, and a PEO/Laponite ratio of 2:1.

Table 1. Major Chemical Composition of the Samples in Weight Percentages

sample	SiO_2 (%)	Al_2O_3 (%)	MgO (%)	TiO_2 (%)	Na_2O (%)	Fe_2O_3 (%)
Laponite[a]	51.10	0.07	23.20	*b*	2.51	
TiO_2 composites prepared:						
without PEO	33.10	0.20	0.61	58.71		0.05
with PEO	55.30	0.12	0.19	43.90		0.02

[a] As received starting reagent without further heating. [b] Not detectable.

in the starting Laponite material, most of the magnesium in the clay platelets was leached out (Table 1). Clearly, a reaction involving the Laponite clay occurred in the synthesis. Such a reaction inevitably results in radical structural changes of the clay layers.

^{29}Si MAS NMR. The profound structural changes occurring in the silicate layers during synthesis are also reflected in the ^{29}Si MAS NMR spectra of the samples (Figure 1).

The ^{29}Si MAS NMR spectrum of Laponite displays two resonance peaks at ≈90 and ≈80 ppm. Such chemical shifts are attributed to the SiO_4 tetrahedra linked with 3 and 2 other SiO_4 tetrahedra (Q^3 and Q^2 sites), respectively. This is expected for the structure of the Laponite clay layer.[19−21] In the clay layer, most SiO_4 tetrahedra are linked to 3 other SiO_4 tetrahedra[20] in Q^3 sites,[21] but the tetrahedra at the edges of the clay layers are linked to 2 other SiO_4 tetrahedra, and thus form the Q^2 sites. The smaller amount of Q^2 sites, compared with that of Q^3 sites, is responsible for the low intensity of the peak at −80 ppm.

The TiO_2 composite samples show a substantially different MAS NMR spectrum. Broad resonance bands in the range from −110 to −80 ppm can be seen, reflecting poor short-range order. The chemical shift at −104 ppm should be assigned to Q^4 sites, where a SiO_4 tetrahedron is linked with 4 other SiO_4 tetrahedra. In the Laponite clay structure there should be no Q^4 sites[19−21] and this is confirmed by the spectrum of the clay. Thus, the Q^4 sites are due to the reaction between Laponite clay and the sol of titanium hydrate of a strong acidity, indicating profound structural changes from the layer structure of the clay. The clay layers do not exist in the reaction products, and this is supported by the chemical analyses (Table 1). Such a mechanism is evidently different from the conventional pillaring process during which the clay retains its layer structure.

TEM Images. Representative TEM images of the pristine Laponite and TiO_2 nanocomposites are compared in Figure 2.

Stringy bundles can be seen in the image of pristine Laponite in Figure 2a. The strings have a uniform thickness of about 1 nm, which is the same as the thickness of the clay layers. Thus, the bundles are clay layers aggregating with poor long-range order. No layered structure can be seen in the image of the TiO_2 nanocomposites. Some residues of the clay layers are observed besides the agglomerates of TiO_2 crystallites in Figure 2b. In Figure 2c, crystallized grains can be seen. The size of the grains is in the range between 3 and 9 nm. These grains are anatase particles because the existence of anatase crystallites with such dimensions is confirmed by the X-ray patterns of the samples. Energy-dispersive X-ray spectroscopy (EDS) was also used to analyze the chemical compositions at different regions over a sample. At least five regions were taken for one sample and the average region size was about 15 nm in diameter. We found no obvious difference from region to region and the overall composition of the sample was uniform, for all samples. This means that, in these samples, TiO_2 and silicate particles are two interdispersed phases on a scale of several nanometers, forming a porous composite structure.

XRD Results. Generally, the intercalated structure of pillared clays can be indicated by the d_{001} peak in the XRD patterns.[11−14] However, it is difficult to observe the peak in the XRD patterns of the starting clay, Laponite, because the clay platelets are small, having a poor long-range order between platelets. In this work, we did not observe a clear peak for the starting clay, Laponite, or a peak for the intercalated layered structure. Furthermore, we could not recognize any crystal form of silica or silicate in the XRD pattern of the samples, although silica accounts for a large portion of the sample mass. The silicate in the samples exists as amorphous particles, but not as clay layers. Characteristic diffraction peaks for anatase with *d*-spacings of 3.6, 2.37, 1.89, and 1.67 Å (2θ values: 25.3, 37.9, 47.6 and 54.8°, respectively) can be clearly observed even from the XRD patterns of the sample before calcination at 773 K (Figure 3). This means that the anatase phase has formed during hydrothermal aging at 373 K.

The mean size of the anatase particles in the calcined samples can be estimated by the broadening of the most intensive X-ray diffraction peak (101) at $2\theta = 25.3°$ using the Debye−Scherrer equation.[15,22] In Table 2, the size of the anatase crystals of TiO_2 nanocomposites

(19) Komarneni, S.; Fyfe, C. A.; Kennedy G. J.; Strobl, H. *J. Am. Ceram. Soc.* **1986**, *69* (3), C45.
(20) Newman, A. C. D. *Chemistry of Clays and Clay Minerals*; Mineralogical Society, Longman Science & Technology: UK, 1987; p 161.
(21) Wilson M. A. *NMR Techniques and Applications in Geochemistry and Soil Chemistry*; Pergamon Press: Oxford, 1987.

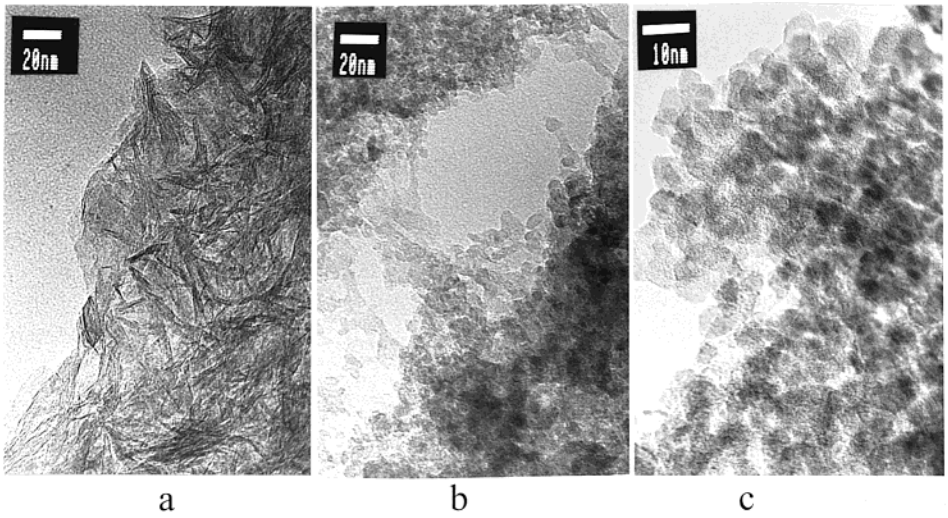

Figure 2. TEM images of Laponite clay (a) and the calcined TiO_2 nanocomposite sample (b and c), the same sample used for Figure 1. Anatase crystals (with texture lines) can be seen in image (c) and the pieces linking the agglomerates of grains in image (b) could be the reaction residues from the Laponite.

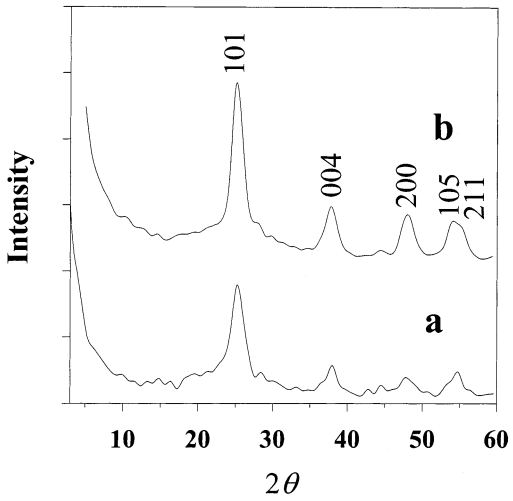

Figure 3. XRD pattern, using Cu Kα radiation, of the TiO_2 nanocomposite in Figure 1 (as the representative of the TiO_2 nanocomposite samples) before and after calcination at 773 K (curves a and b, respectively). The peaks observed at 25.3, 37.9, 47.6, and 54.8° 2θ are characteristic diffraction peaks for anatase.

Table 2. Influence of the Acidity in the Sol Solution on the Crystal Size of Anatase in TiO_2 Composite Samples[a]

prepared without PEO			prepared with PEO		
H^+/Ti	crystal size (nm)	pore size (nm)	H^+/Ti	crystal size (nm)	pore size (nm)
2	3.65	4.14	2	3.54	4.83
4	5.15	4.72	4	3.93	5.02
8	8.96	6.38	8	5.46	5.19

[a] The mean pore size of the samples calculated using the adsorption data is also given for comparison.

samples, which were prepared using the sol solution, are recorded for various molar ratios of acid to titanium (H^+/Ti). We found that when the amounts of clay and surfactant in the synthesis were kept constant, the crystal size in the samples increased from 3.65 to 8.96 nm as the H^+/Ti ratio was increased from 2.0 to 8.0. Thus, one can alter the size of the anatase particles in the products by manipulating various synthesis parameters, such as the acidity of the sol solution. This is of significant importance because we can effectively tailor the structure of these solids for various applications.

It is also noted that the mean pore diameter of the samples, derived from the nitrogen adsorption data using the *t*-plot method,[18,23] is of a similar dimension to the anatase particle size and varies in the same trend as the particle size. This implies that the pores in the samples are the voids between the anatase nanocrystals. Besides, the crystal size is also smaller for the PEO samples (Table 2). The PEO surfactant micelles are dispersed among the nanoparticles of TiO_2 and silicate and, thus, separate the TiO_2 nanoparticles apart. These particles have less chance to agglomerate into large particles so that the TiO_2 nanoparticles in the PEO sample are smaller, compared to those in the corresponding surfactant-free sample. This could also be the reason for the sizes of pores and particles of the PEO samples being less dependent on the H^+/Ti ratio.

N_2 Adsorption Data. The nitrogen adsorption capacity of a solid reflects its porosity.[23] Three adsorption and desorption isotherms are presented in Figure 4. The pore structure information can be derived from the nitrogen adsorption data so that we can specify the location of the surfactant in the nanocomposite as prepared by comparing the pore structures of the sample before and after calcination.

The amount of adsorption by the uncalcined sample (isotherm a) is very low. The calcination at 773 K brings about a pronounced increase in the porosity of the sample and, thus, in adsorption. During heating, the samples dehydrate and the surfactant was removed as indicated by the TGA results (discussed later), leaving a large number of pores in the sample. Comparison of isotherm c with isotherm b indicates clearly that introducing the PEO surfactant greatly increases the porosity of the composite samples. Isotherm c has the shape of a Type IV isotherm, which is characteristic of mesoporous solids.[23] N_2 isotherms of other samples

(22) Ding, Z.; Zhu, H. Y.; Lu, G. Q.; Greenfield, P. F. *J. Colloid Interface Sci*. **2001**, *238*, 267.-

(23) Gregg, S. J.; Sing, K. S. W. *Adsorption, Surface Area and Porosity*, 2nd ed.; Academic Press: New York, 1982.

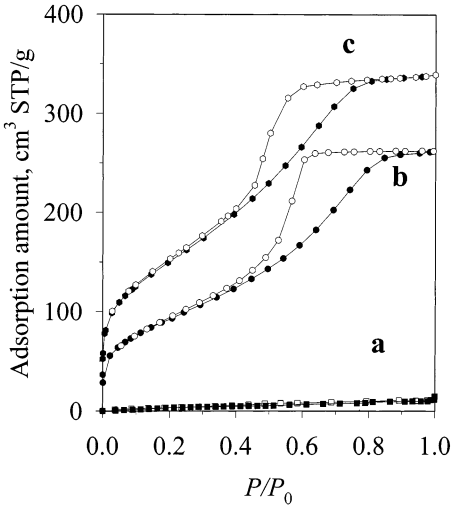

Figure 4. Adsorption and desorption isotherms of TiO_2 nanocomposite samples. Curve a is for an uncalcined TiO_2 nanocomposite prepared with PEO surfactant Tergitol 15S-12, a [Ti]/[H^+] ratio of 1:4, and a PEO/Laponite ratio of 2:1. The sample was degassed at 383 K, at which temperature the surfactant would not be removed from the sample. Curve b is for a calcined sample prepared at the same conditions as for the sample of curve a, but using no surfactant. Curve c is for the sample of curve a following the calcination, after the surfactant had been completed removed.

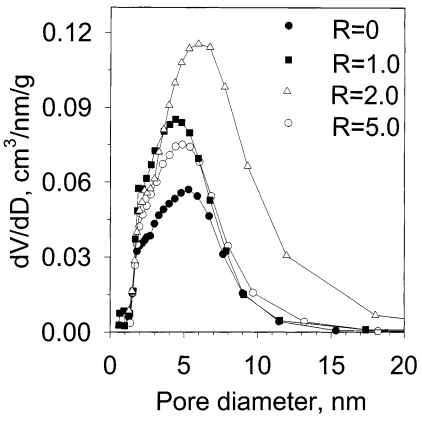

Figure 5. Influence of the PEO/Laponite ratio, *R*, on the pore size distribution (PSD) of calcined TiO_2 nanocomposite samples. All samples were prepared with PEO surfactant Tergitol 15S-7. The PSDs were calculated from the N_2 isotherms.

prepared with surfactants are similar to isotherm c in shape.

To clearly illustrate the influence of the surfactant properties on the structure of the calcined products, pore size distributions (PSDs) of some samples were calculated from the N_2 isotherms and are given in Figure 5.

As the PEO/clay ratio *R* in the synthesis increases, pore volume (as indicated by the area under the PSD curve) initially increases (Figure 5) before reaching a maximum at a ratio of 2 and then decreasing.

Surprisingly, data in Table 3 demonstrate clearly that the mean pore size of the samples decreases with the number, *n*, of ethylene oxide groups ($-CH_2CH_2O-$) in a PEO surfactant. In the preparation of these samples, a constant weight of surfactant (8 g), with molecular weights from 420 to about 1520, was used. According to the general formula for this class of surfactants, the molecular weight and the dimension of a surfactant molecule increases with the number of the ethylene oxide groups in the surfactant. In the templating mechanism, the pore size of the product increases with the molecular size of the surfactant.[7−10,24,25] However, for the PEO surfactants used in this study the trend appears quite different.

Table 3. Influence of the Molecular Size of the Surfactants as Given by *n* (Number of Ethylene Oxide Groups) on the Surface Area (S_{BET}), Pore Volume (V_t), and Mean Pore Size (*d*) of the Calcined TiO_2 Nanocomposite Samples

	S_{BET} (m^2/g)	V_t (cm^3/g)	*d* (nm)
n =			
5	514	0.616	6.86
7	627	0.741	5.27
9	747	0.651	4.76
12	525	0.508	4.10
30	459	0.481	4.34

Most pores in the calcined solids are in a range between 3 and 9 nm, which is much larger than the molecular sizes of the surfactants. Hence, pores are not created by a single surfactant molecule. PEO surfactants of similar molecular formula were found to form rodlike or wormlike micelles with a diameter of about 6 nm in aqueous solution.[26] Thus, in our synthesis approach the surfactants should exist in micelles. The surfactant micelles dispersed in the composite structure can separate the hydrolyzed sol particles, preventing them from sintering during the drying and heating procedures.

All the surfactants used had the same alkyl chain with the only difference between them being the number of ether groups, $(CH_2CH_2O)_n$, present. When the surfactant is dispersed in a polar media, such as in aqueous systems or polar surfaces, the oxide groups would form the outer surface of the micelles and would be in contact with the polar media [27−29] which, in this case, is the surface of sol particles. The ether groups $(CH_2CH_2O)_n$ of the surfactant can interact with the surfaces of metal hydroxide through hydrogen bonding.[30,31] A surfactant with large *n* is expected to have a much stronger interaction with the precursor surface when compared to a surfactant with small *n*. This could be the reason for the observation that the mean pore diameter decreases with *n*: the stronger interaction results in micelles of a smaller diameter.

Thermogravimetric Analysis. The weight losses of the samples during the course of calcination in air up to 1173 K are shown in Figures 6 and 7.

The sample prepared without surfactant loses about 15% of its weight below 420 K mainly due to dehydration (Figure 6). In contrast, the weight loss below this temperature for samples prepared with PEO surfactant is relatively small (Figures 6 and 7) below 5%. This

(24) Huo, Q.; Margolese, D. I.; Ciesla, U.; Feng, P.; Gier, T. E.; Sieger, P.; Leon, R.; Petroff, P. M.; Schüth, F.; Stucky, G. D. *Nature* **1994**, *368*, 317.
(25) Ying, J. Y.; Mehnert, C. P.; Wong, M. S. *Angew. Chem., Int. Ed.* **1999**, *38* (1/2), 56.
(26) Lin, Z.; Scriven, L. E.; Davis, H. T. *Langmuir* **1992**, *8*, 2200.
(27) Cummins, P. G.; Hayter, J. B.; Pemfold, J.; Staples, E. *Chem. Phys. Lett.* **1987**, *138*, 436.
(28) Cummins, P. G.; Staples, E.; Pemfold, J. *Langmuir* **1989**, *5*, 1195.
(29) Penfold, J.; Staples, E.; Cummins, P. G. *Adv. Colloid Interface Sci.* **1991**, *34*, 451
(30) Michot, L. J.; Barrès, O.; Hegg, E. L.; Pinnavaia, T. J. *Langmuir* **1993**, *9*, 1794.
(31) Zhu, H. Y.; Lu, G. Q. *Langmuir* **2001**, *17*, 588.

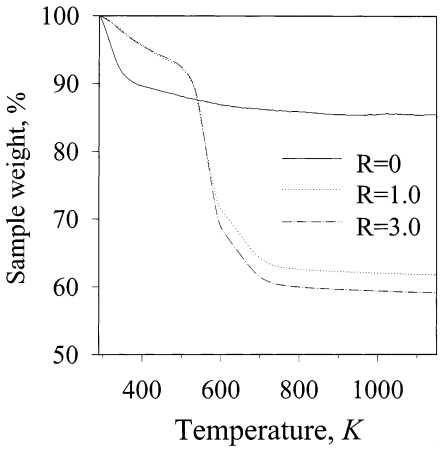

Figure 6. Weight losses of the TiO_2 nanocomposite samples during the course of heating to 1173 K in air. The samples were prepared with the surfactant Tergitol 15S-7, but with different PEO/Laponite ratios (*R*).

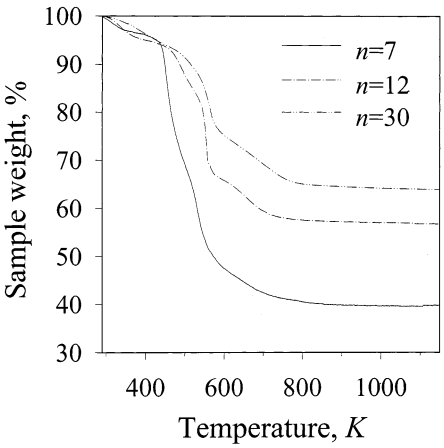

Figure 7. Weight losses of the samples during the course of heating in air up to 1173 K. The samples were prepared using different PEO surfactants, but the same PEO/Laponite ratio (2:1) and the $[Ti]/[H^+]$ ratio (1:4).

suggests that the samples prepared with surfactant have much lower water contents. However, for these samples a sharp weight loss of about 20−50% is observed in the temperature range between 500 and 600 K, whereas a loss of only 9% was recorded for the reference sample in the same temperature range.

Figure 7 also shows that as *n* increases, the sharp weight loss commences at higher temperatures. The boiling point of the surfactant increases with the number of ethylene oxide groups in the molecule, *n*. Therefore, this sharp weight loss is mainly attributed to the evaporation of the surfactants. It was observed that a large amount of surfactant is released over a temperature range 473−573 K during calcination. The interaction of the surfactant micelles with the surface of the sol particles most likely occurs by hydrogen bonding, which is much weaker than Coulombic interactions. This weaker bonding suggests that the surfactants were removed by evaporation during heating rather than by pyrolysis. This means that the surfactants used may be collected simply by a cooling trap and reused.

In Figure 8, the weight loss below 773 K, obtained from TGA analysis, is plotted against the pore volume of the calcined products.

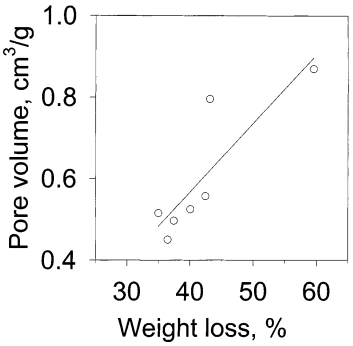

Figure 8. Relation between the weight loss below 773 K and the volume of the framework pores in the calcined products.

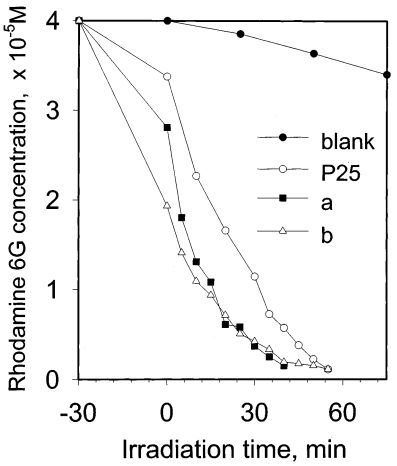

Figure 9. Catalytic performances of the samples for photodegradation of Rhodamine 6G. Curves a and b illustrate the performance of two TiO_2 nanocomposite samples listed in Table 1 (a is for the sample prepared without surfactant and b for the sample prepared with the surfactant).

The pore volume increases with weight loss and a linear relation is evident. Mesopores in the samples clearly arise from the removal of water and surfactant species. In addition, according to the TGA analysis, the surfactants account for one-third to one-half of the mass of the dried samples. Therefore, the large porosity is primarily due to the presence of the surfactants where they acted as space filler.

Photocatalytic Performance. The catalytic performance of the TiO_2 nanocomposite samples for photodegradation of Rhodamine 6G under UV light at ambient temperature is shown in Figure 9. The performance of a commercial titanium dioxide P25 is also given in the figure for comparison. The overall photocatalytic efficiency of the two TiO_2 nanocomposite samples is comparable to that of P25, which is known to be the best commercial photocatalyst of pure TiO_2. Here, TiO_2 accounts for about one-half of the sample mass of the nanocomposite samples (Table 1). Therefore, the activity per mass of TiO_2 for these samples is superior. Moreover, the nanocomposite samples can be readily separated from the suspension after the reaction because they sedimented in minutes when the stirring was stopped, while the P25 sample could not sediment over hours, and penetrated the filtration paper when the suspension was filtered. This could lead to a potential difficulty in downstream separation.[6] The size of TiO_2 particles in the nanocomposite samples is much smaller, compared with that of the P25 power. But these small

particles are linked by silicate particles to form large granules, which can be recovered easily from aqueous solutions by filtration or sedimentation. This is an important advantage in practice.

One may also note that before the UV light was switched on (the region on the left-hand side of the point zero on the time axis in Figure 9), the concentration of Rhodamine 6G was substantially below 4×10^{-5} M for all the samples. This is due to adsorption of Rhodamine 6G by the catalysts. The BET surface area of P25 is about 50 m^2/g, while the samples for curves a and b have surface areas of over 300 and 600 m^2/g, respectively. With such large surface areas, the composite samples exhibit a binary function for removing organic compounds from water through both photocatalysis and adsorption. This could be a useful property for their environmental application.

Discussion

Reaction. The reaction between the clay suspension and acidic pillaring solutions has generally been ignored in earlier studies. The clay layers have been regarded as inert with respect to reaction and almost intact in terms of chemical composition through the pillaring process. Nonetheless, layered clays can react with various acids even under moderate conditions.[32−34] Acid leaching is regarded as an effective means to activate clays. The acid leaching is known to result in considerable changes in the composition and structure of the clay layers. Broad d_{001} peaks have often been observed in the XRD pattern of TiO_2 pillared clays.[11,12] The broad peak could result from partially acid-leached clay layers. The pillaring solution was generally obtained by hydrolysis of a titanium salt or a titanium alkoxide in acid solution[12,15] and, thus, is of strong acidity. In some studies, the d_{001} peaks cannot even be observed.[15,35]

On the other hand, the dispersion of Laponite exhibited a high pH. It is known that an increase in the pH of a solution will lead to polymerization of the sol particles in the solution.[36] Therefore, mixing the Laponite dispersion with the sol solution inevitably induces further hydrolysis of the sol particles, such that large precursors of TiO_2 nanoparticles are formed. This is an important reason we chose Laponite as the starting clay. The precursor species of the TiO_2 nanoparticles most likely condense on the acid-leached silicate particles surrounding them. During subsequent hydrothermal aging, fine anatase particles form from the condensed sol particles. In later heating, we see the growth of anatase particles (indicated by the sharp [101] peak in the XRD pattern) accompanied by dehydration or dehydroxylation (indicated by the weight loss above 600 K in Figures 6 and 7). A composite structure with large porosity forms in which nanoparticles of anatase and silicate, in the size range of several nanometers, disperse homogeneously among each other.

Structural Features. The structure of the TiO_2 nanocomposite solids is profoundly different from a pillared layered structure. The pillared layered clays are microporous solids (pore size below 2 nm) with a moderate porosity. The conventional TiO_2 pillared clays have a pore volume between 0.15 and 0.40 cm^3/g and a BET surface area between 200 and 350 m^2/g.[11,12,15,35] In comparison, the nanocomposites are mesoporous solids and exhibit much larger surface area and pore volume (Table 3).

As shown above, introducing surfactants during the synthesis leads to pronounced increases in the BET surface area and pore volume of the calcined products. In addition, as shown in Table 2, the size of the anatase particles in the calcined products depended strongly on the acidity of the sol solution, independent of use of the PEO surfactant. This provides us with a useful means for tailoring the nanocomposite structure for different applications. During the last 2 decades applications of pillared clays as catalysts or catalyst supports for numerous chemical reactions have been attempted.[37] In general, a larger specific surface area, pore volume, and pore size, and better acidic characteristics, are required to improve the effectiveness of a catalyst. With respect to these properties, the TiO_2 nanocomposites of the present study are obviously superior to the TiO_2 pillared clays and, therefore, have a greater potential to be adopted for catalytic applications.

Photocatalytic Performance. A crystallite form of TiO_2, in an anatase or rutile phase, is necessary for an efficient photocatalyst.[38] Most titanium dioxide in TiO_2 pillared clays prepared by conventional pillaring techniques are amorphous so that the pillared clays have exhibited poor activity for the photodegradation of phenol in water.[15] The TiO_2 pillars are too small to form a crystal phase and it is also extremely difficult to control the pillar size in the conventional pillaring process. The TiO_2 nanocomposite samples are superior to TiO_2 pillared clays due to the crystal particles of TiO_2 and large porosity.

The superior catalytic performance of the TiO_2 nanocomposites can also be attributed to the smaller size (3−9 nm) of the TiO_2 crystals in the samples compared to that in P25 (about 25 nm). First, the small particles have a larger specific surface area of TiO_2 on which the photocatalytic reaction takes place. Catalysts with a large specific surface area are expected to demonstrate higher catalytic activity. Second, it has been reported that as the TiO_2 crystals become smaller, especially below 10 nm, their catalytic performance increases remarkably.[39] Apart from the physical properties, such as surface area, the "size quantization effect"[39] could play an important role for good photocatalytic activity of catalysts with TiO_2 particles of several nanometers only.

Conclusions

In this work, we have proposed and tested a new synthesis strategy for constructing highly porous com-

(32) Corma, A.; Mifsud, A.; Sanz, E. *Clay Miner.* **1987**, *22* (2), 225.
(33) Mokaya, R.; Jones, W. *J. Catal.* **1995**, *153* (1), 76.
(34) Kaviratna, H.; Pinnavaia, T. J. *Clays Clay Miner.* **1994**, *42* (6), 717.
(35) Occelli, L.; Peaden, P. A.; Ritz, G. P.; Iyer, P. S.; Yokoyama, M. *Microporous Mater.* **1993**, *1*, 99.
(36) Baes, C. F.; Mesmer, R. E. *The Hydrolysis of Cations*; John Wiley & Sons: New York, 1986.
(37) Gil. A.; Gandia, L. M.; Vicente, M. A. *Catal. Rev.* **2000**, *42* (1/2), 145.
(38) Ooka, C.; Akita, S.; Ohashi, Y.; Horiuchi, T.; Suzuki, Ki.; Komai, S.; Yoshida, H.; Hattori, T. *J. Mater. Chem.* **1999**, *9* (11), 2943.
(39) Anpo, M.; Shima, T.; Kodama, S.; Kubokawa, Y. *J. Phys. Chem.* **1987**, *91*, 4305.

posite structures of anatase and silicate nanoparticles from aqueous systems. The starting materials, clay platelets and sol particles of titanium hydrate, react with each other. Consequently, the clay platelets are acid-leached and converted to amorphous silicate fragments and polymerized sol particles, the precursors of anatase nanopaticles condensed on the silicates. Introducing PEO surfactants in the synthesis leads to a significant increase in the specific surface area and pore volume of the calcined products. The surfactant molecules form micelles that have strong affinity to the surfaces of both precursors and clay and act as a space filler. The anatase crystals form during hydrothermal aging and the crystals grow in the subsequent heating process. It appears that the surfactants were evaporated rather than lost by pyrolysis during heating. This feature brings about economical and environmental advantages to the synthesis. The calcined solids obtained have a highly porous structure in which nanoparticles of anatase and silicate are well-dispersed among each other. We can readily alter the size of the anatase particles and their porosity in the sample by manipulating the synthesis parameters. With smaller sizes of TiO_2 crystals and a larger porosity, the TiO_2 nanocomposites exhibited superior properties as photocatalysts for the degradation of Rhodamine 6G in an aqueous solution.

Acknowledgment. Financial support from the Australian Research Council (ARC) are gratefully acknowledged. H.Y.Z. is also indebted to the ARC for the QE II fellowship. Thanks also go to Ms. Xiuquan Yan for conducting part of the experimental work.

CM0205884